ADVANCES IN ATMOSPHERIC SCIENCES, VOL. 23, NO. 1, 2006, 1–13

Comparison of TRMM and Water District Rain Rates over New Mexico

Long S. CHIU*[1,2], Zhong LIU[1,2], Jearanai VONGSAARD[2,4], Stanley MORAIN[3], Amy BUDGE[3], Paul NEVILLE[3], and Chandra BALES[3]

[1] *NASA/Goddard Space Flight Center, Distributed Active Archive Center, Greenbelt, Maryland* 20771, *USA*

[2] *Center for Earth Observing and Space Research, School of Computational Sciences, George Mason University, Fairfax, Virginia* 22030-4444, *USA*

[3] *Earth Data Analysis Center, University of New Mexico, Albuquerque, New Mexico* 87131, *USA*

[4] *Thai Royal Military Academy, Bangkok, Thailand*

(Received 20 January 2005; revised 4 July 2005)

ABSTRACT

This paper compares monthly and seasonal rain rates derived from the Version 5 (V5) and Version 6 (V6) TRMM Precipitation Radar (TPR, TSDIS reference 2A25), TRMM Microwave Imager (TMI, 2A12), TRMM Combined Instrument (TCI, 2B31), TRMM calibrated IR rain estimates (3B42) and TRMM merged gauge and satellite analysis (3B43) algorithms over New Mexico (NM) with rain gauge analyses provided by the New Mexico water districts (WD). The average rain rates over the NM region for 1998–2002 are 0.91 mm d^{-1} for WD and 0.75, 1.38, 1.49, 1.27, and 1.07 mm d^{-1} for V5 3B43, 3B42, TMI, PR and TCA; and 0.74, 1.38, 0.87 and 0.97 mm d^{-1} for V6 3B43, TMI, TPR and TCA, respectively. Comparison of V5 3B43 with WD rain rates and the daily TRMM mission index (TPR and TMI) suggests that the low bias of V5 3B43 for the wet months (summer to early fall) may be due to the non-inclusion of some rain events in the operational gauge analyses that are used in the production of V5 3B43. Correlation analyses show that the WD rain rates vary in phase, with higher correlation between neighboring WDs. High temporal correlations (>0.8) exist between WD and the combined algorithms (3B42, 3B43 and TCA for both V5 and V6) while satellite instrument algorithms (PR, TMI and TCI) are correlated best among themselves at the monthly scale. Paired t-tests of the monthly time series show that V5 3B42 and TMI are statistically different from the WD rain rates while no significant difference exists between WD and the other products. The agreements between the TRMM satellite and WD gauge estimates are best for the spring and fall and worst for winter and summer. The reduction in V6 TMI (−7.4%) and TPR (−31%) rain rates (compared to V5) results in better agreement between WD estimates and TMI in winter and TPR during summer.

Key words: satellite precipitation, TRMM, Water District, New Mexico, surface rain

1. Introduction

Accurate rainfall measurements are crucial to many hydrological and environmental applications. Rain gauge networks have been the basic measuring units for measuring rainfall events. Most hydrological models have been calibrated against gauge measurements. Over the continental U. S., the network of NEXRAD radars established in the mid 1990s provides much improved coverage, yet the problems of inter-radar calibration, blockage by mountains, and gaps between radar coverage areas still limit its capability (Young et al., 1999). Geosynchronous satellites provide almost continuous coverage, yet rain estimates from visible or infrared measurements are considered indirect estimates. Microwave measurements taken onboard low Earth orbit or polar orbit satellites are deemed to be the more physical approach. A combination of gauge, radar and satellite measurements is ultimately needed for improved space/time rainfall estimation.

*E-mail: lchiu@gmu.edu

The Tropical Rainfall Measuring Mission (TRMM), jointly sponsored by the National Aeronautics and Space Administration (NASA) of the U. S. and the Japan Aerospace Exploration Agency (JAXA, previously known as the National Space Development Agency, or NASDA), is the first coordinated international satellite mission to monitor and study tropical and subtropical rain systems (Simpson et al., 1988). A detail description of the TRMM sensor package and algorithms is given by Kummerow et al. (1998). The TRMM rain sensor package includes the first space-borne Precipitation Radar (TPR), a TRMM Microwave Imager (TMI) and a Visible and Infrared Scanner (VIRS). The TRMM data have gone through a few major reprocessing cycles, as improved knowledge of the sensors and algorithms leads to better sensor calibration and algorithms. Version 5 (V5) has shown significant improvement over the previous version of data (Kummerow et al., 2000). Over land, Shin et al. (2001) showed that TMI rainfall estimates are higher than PR in the TRMM domain (35°N–35°S) for the first two years of TRMM data. Adler et al. (2003) pointed out that there is a distinct reversal of the algorithm bias between the tropics and the subtropics. While global differences between the TRMM satellite estimates are of the order of 20%, there are large regional differences (Kummerow et al., 2000; Adler et al., 2003). Chiu et al. (2005b) used a paired t-test to compare TPR and TMI rain rates using six years of data. They showed that over the continental U. S. within the TRMM domain, TMI is higher than PR in the western U. S. while PR is higher in the eastern half over the year. This pattern is fairly persistent over the year. However, there is a slight reversal in the summer season. Version 6 (V6) algorithms are used for processing starting April 2002. Substantial modifications have been implemented in the V6 TMI and TPR algorithms. Both V5 and V6 data are used in our study to show the improvement in the V6 over the V5 algorithms.

In the dry SW region of the U. S., rainfall is an important component in the water budget. Monitoring the water budget has large environmental and geopolitical implications. In the Rio Grande regions, for example, water pacts mandate that a certain fraction of water from the Rio Grande River should be released to the downstream regions, and water rights have to be traded to ensure adequate water resources for city development and rural expansion.

New Mexico is situated in a mountainous and dry region: the annual rainfall in Albuquerque is about 200 mm (Rudloff, 1981), with an average of 40 rain days per year. Because of the scarcity of rain events, this region will provide a stringent test for the TRMM algorithms.

Gauge estimates are not the "ground truth" of surface precipitation. They suffer from measurement errors (Sevruk, 1986). However, it is important to quantify the biases of satellite algorithms relative to the gauge estimates since most hydrologic models are calibrated against rain gauge measurements.

2. Data

The processing flow of the TRMM satellite algorithms is available from the DAAC web site (http://daac.gsfc.nasa.gov/hydrology/TRMM_v6.shtml). Over land, there are three TRMM level 2 surface rain rate products and five Level 3 products. Level 2 products are geophysical parameters in satellite orbit coordinates, and Level 3 and higher level products represent space/time average products.

2.1 *V5 algorithms*

We will focus on the level 2 TRMM Microwave Imager Hydrometeor Profile (TMI, TSDIS reference 2A12), TRMM Precipitation Radar Profile (TPR or 2A25), and TRMM Combined Instrument Algorithm (TCA, 2B31), and the level 3 TRMM Adjusted Merged Infrared Precipitation (3B42) and the TRMM and Other Satellite Precipitation (3B43). TMI and TPR are the main rain sensors in the TRMM rain package. TCA is a merged algorithm from TMI and PR. The TCA is then calibrated with VIRS and the calibration applied to geosynchronous satellite infrared data to form the V5 daily 3B42 product. 3B42 is then merged with gauge analysis to produce the 3B43 product.

Table 1 shows the characteristics of the TRMM products used in this study. The TMI Hydrometeor Profile (TSDIS reference 2A21) rain rate is retrieved from the brightness temperature data observed by the TMI channels. The algorithm performs Bayesian retrievals by selecting the most probable rainfall profile from the algorithm database that is consistent with the TMI brightness temperature observations. The database of rainfall profiles is based on output of cloud resolving models, such as the Goddard Cloud Ensemble Model (Kummerow et al., 2001).

The TPR profile algorithm (2A25) calculates the vertical rain profile from the estimated reflectivity profile by using an appropriate reflectivity-rain rate (Z-R) relationship. A drop size distribution is assumed. No attenuation correction is performed at low rain rates. At high rain rates, attenuation due to rain is corrected. The attenuation-reflectivity relationship is adjusted to relfect the dependency on the raindrop size distribution and other environmental conditions. The algorithm is described in detail in Iguchi et al. (2000).

The TCA calculates the vertical structure of rainfall (rates and drop-size-distribution parameters)

Table 1. Characteristics of TRMM algorithms used in this study.

TSDIS Ref. #	Algorithm Name	V5 characteristics	Relevant V6 changes
2A12	TMI Hydrometeor Profile	Bayesian retrieval based on Cloud Resolving Model	Separate algorithms for land/ocean/coast; improved land mask
2A25	TPR Rain Profile	Hybrid of Hitschfeld-Bordan and surface reference method; calculates rain profile using appropriate Z-R relation	Water vapor, cloud liquid water and molecular oxygen attenuation included, estimation of surface rain rate
2B31	TRMM Combined (TCA) Rainfall Profile	Retrieves optimal drop size distribution and sharp parameters that best match TPR reflectivity and TMI brightness temperature distribution	No change
3B42	TRMM and Other-GPI Calibration Rainfall	Daily 1 degree calibrated geosynchronous IR rain rate using TRMM estimates	3-hourly 0.25 degree all available microwave-IR estimates scaled to 3B43 monthly total
3B43	TRMM and Other Sources Rainfall	Monthly 1 degree merged rain rate from TRMM, geosynchronous IR, SSM/I, rain gauges	Monthly 0.25 degree merged rain rate from monthly 3B42 and gauge analyses

based upon the TMI and the TPR within the TPR swath. The algorithm retrieves the optimal drop size distribution and shape parameters that best match the PR reflectivity profile. The brightness temperature distribution associated with the PR profile is then calculated using a radiative transfer model. The calculated brightness temperature distribution is then matched to the observed TMI microwave brightness temperature distribution (Haddad et al., 1997a, b).

The algorithm 3B-42 produces TRMM-adjusted merged-infrared (IR) daily precipitation and root-mean-square (RMS) precipitation-error estimates at a spatial resolution of $1^\circ \times 1^\circ$. Two calibrations are performed. First, the wide swath TMI data are calibrated to the narrow swath TCA (TPR) data. Coincident VIRS and TMI data are gridded and accumulated monthly. The monthly gridded VIRS swath data are then calibrated to the TCA data via a TMI-TCA relation. Using the monthly average coincident VIRS and TMI rain data (calibrated using TCA), IR calibration parameters are computed. These IR calibration parameters are then applied to the spatially and temporally ($\sim$3 hourly) merged-IR data from geosynchronous satellite data to produce the TRMM-adjusted merged-IR precipitation. (Huffman et al., 1997). When applying the VIRS-TCA calibration, some of the pixels produce unrealistic values. These pixels are set to zero.

The gridded $1^\circ \times 1^\circ$ monthly 3B43 rain estimates are produced by merging the monthly accumulation of daily 3B-42 and the monthly rainfall from the Climate Assessment and Monitoring System (CAMS) or Global Precipitation Climatology Centre (GPCC) rain gauge analysis (Rudolf et al., 1994). In the merging of these datasets, they are weighted by the inverse of their respective random error fields (Huffman et al., 1997).

2.2 *V6 algorithms*

The V6 TMI algorithm consists of three distinct algorithms depending on the surface type, viz., ocean, land, or coast. A key change is an improved surface type mask from a 25 km grid (V5) to a 1/6 degree (V6) land mask. The TPR algorithm processing has undergone significant changes. The Level-1 TPR radar-received power that converts instrument counts to echo power was changed resulting in an effective increase in echo strength of 0.35 dBm. This corresponds to an increase in TPR reflectivity, and hence an increase in TPR rainfall. Additionally, attenuation due to water vapor, cloud liquid water and molecular oxygen are now included in V6 TPR. The most significant change, however, is the estimation of attenuation below the clutter level using prescribed reflectivity slopes. This results in the addition of an estimated surface rainfall rate (at the Earth's ellipsoid) in V6 compared to

the near surface rainfall rate (above the clutter) in V5. This distinction is significant since the height at which the near surface rainfall is reported is a function of the incidence angle, generally closer to the Earth's ellipsoid near nadir and up to 2 km above the ellipsoid at the scan edges. The reflectivity slopes used for getting below the clutter rainfall depend on the surface and precipitation type (Meneghini et al., 2004). This approach incorporates the effect of raindrop evaporation below the cloud base, thus mitigating the effect of virga, which may be prevalent over continental dry regions in the summertime.

The V6 3B42 is a 3-hourly 0.25° product based on multi-satellite precipitation analysis (MPA, Huffman et al., 1997, 2001, 2004). First, all available 3-hourly microwave-IR combination estimates are put into the appropriate space/time bin. These high-resolution data are summed over a calendar month to create a monthly multi-satellite product. The multi-satellite and gauge analysis are merged optimally to create a post-real-time monthly satellite-gauge product, which is the V6 TRMM product 3B43. V6 3B42 is then scaled as the ratio of monthly multi-satellite to 3B43 [the scale factor being limited to the range (0.2, 2)]. There is no gauge analysis at the 0.25° scale, hence 3B43 spatial variability less than 1° is introduced by the MPA. There is no significant difference between the V6 monthly 3B42 and the 3B43 product (Chiu et al., 2005b).

2.3 *Data preprocessing*

Both the daily (3-hourly) 3B42 and monthly 3B43 data are standard TRMM products. Monthly 3B42 data are computed from the daily (3 hourly) data. The GSFC DAAC binned the TMI and TCA swath data into 0.5° and 0.25° grids, respectively (Chiu et al., 2005a). TSDIS developed a gridded product 3G68 which contains TMI, TPR and TCA data binned to 0.5° boxes. Monthly means of TMI, TPR and TCA are computed from 3G68.

2.4 *Gauge data*

Water divisions in the U. S. are contiguous areas within a state that have fairly homogeneous hydrological conditions. Within each state, the water divisions occupy roughly equal area and there are at least 5–10 rain gauges within each water division. The analyzed monthly rainfall data within each WD are available from NCDC via the following web site: http://lwf.ncdc.noaa.gov/oa/climate/onlineprod/drought/ main.html. Another source of gauge analysis is the Global Precipitation Climatology Centre (GPCC) monitoring analysis available from the GPCC web site (http://www.dwd.de/en/FundE/Klima/KLIS/int/GPCC/). The average number of GPCC gauges for this region is roughly 10 gauges before July 2001 and 20 afterwards.

3. Analysis and results

Figure 1 shows the water divisions (WDs) in New Mexico and rainfall accumulation at each WD over five years (January 1998- December 2002). There is a tendency for higher rainfall accumulation towards the northeast. Figure 2 shows the WD data for 2000 for the eight WDs. The WD rainfall tends to vary in phase. Table 2 shows the correlation of monthly rain rates between the WDs. Neighboring WDs tends to show higher correlations. For example, the correlation between WD five (WD-5) and neighboring WDs are 0.94 (with WD-4), 0.91 (with WD-6), 0.88 (with WD-2), 0.87 (WD-1), 0.86 (WD-8), and 0.76 (WD-3) and 0.64 (WD-7).

3.1 *V5 results*

Figure 3 shows the five-year rainfall accumulation of 3B42 and 3B43. This figure was produced using a modified version of the TRMM On-line Visualization and Analysis (TOVAS, http://lake.nascom.nasa.gov/tovas/) package (Chiu et al., 2005a; Liu et al., 2003). The TOVAS allows visualization and analysis of selected rainfall products over the web, and is convenient for quick display and analysis.

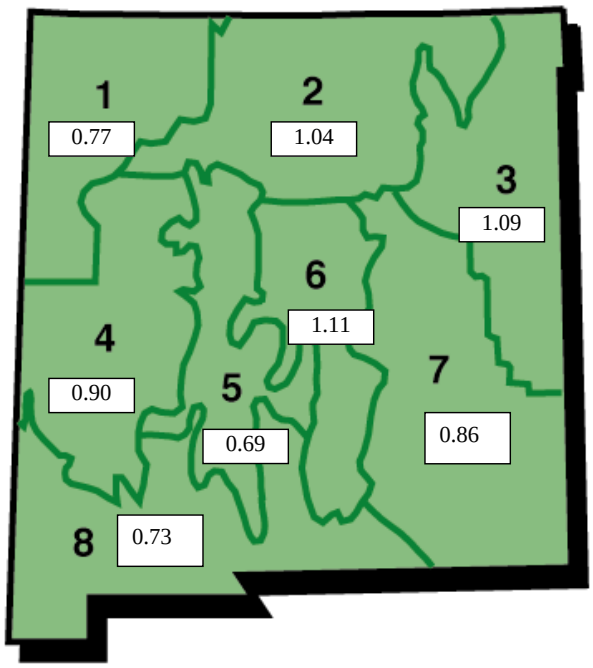

Fig. 1. Average daily rainfall over the New Mexico Water Districts (1998–2002). Units: mm d^{-1}.

Table 2. Temporal correlations between New Mexico Water District (WD) monthly rain rates (1998–2002).

	WD-1	WD-2	WD-3	WD-4	WD-5	WD-6	WD-7
WD-2	0.89	1.00					
WD-3	0.71	0.87	1.00				
WD-4	0.86	0.86	0.71	1.00			
WD-5	0.87	0.88	0.76	0.94	1.00		
WD-6	0.77	0.86	0.78	0.90	0.91	1.00	
WD-7	0.56	0.73	0.86	0.63	0.64	0.77	1.00
WD-8	0.74	0.77	0.65	0.88	0.86	0.91	0.71

Table 3. Temporal correlation between TRMM algorithm monthly rain rate estimates (1998–2002) over the New Mexico region. V6 results appear in parentheses.

Algorithm	WD	3B42 V5	3B43	TMI	TPR	TCA
mean (mm d^{-1})	0.91	1.38	0.75 (0.74)	1.459 (1.38)	1.27 (0.87)	1.07 (0.97)
3B42	0.81					
3B43	0.88 (0.97)	0.74				
TMI	0.66 (0.71)	0.73	0.62 (0.66)			
TPR	0.76 (0.81)	0.79	0.68 (0.78)	0.85 (0.95)		
TCA	0.80 (0.81)	0.80	0.71 (0.78)	0.86 (0.95)	0.99 (0.99)	1.00

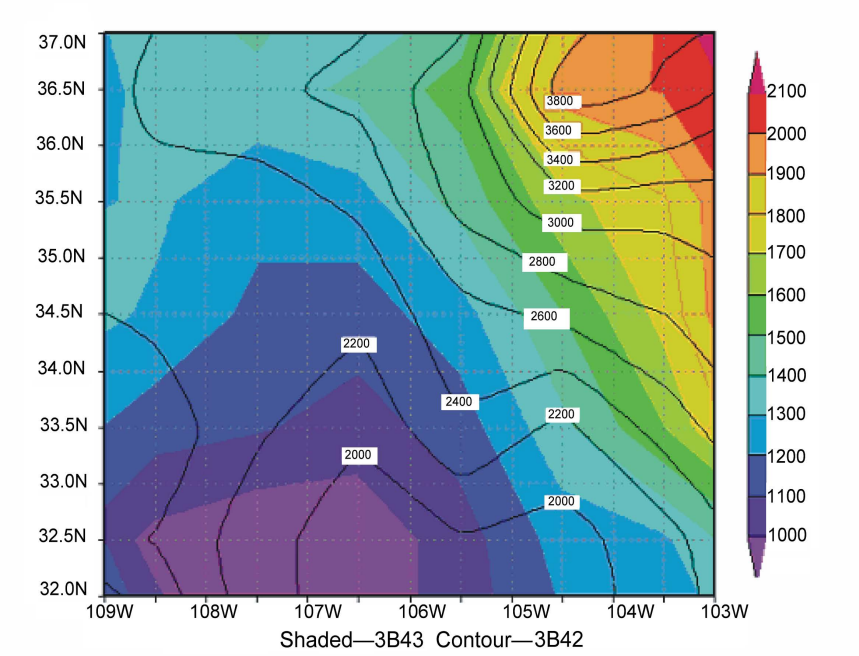

Fig. 2. Five-year (January 1998–December 2002) rainfall accumulation over New Mexico estimated from the TRMM 3B42 and 3B43 products. (Units: mm)

The general spatial patterns of rainfall accumulation of 342 and 3B43 are similar to those of the WDs. There are major differences between 3B42 and 3B43, however. The minimum in 3B43 is shifted slightly to the west of that of 3B42. 3B42 also shows higher rain rates, particularly in the northeast corner.

Monthly mean rain rates for TMI, TPR and TCA are computed from 3G68 over the region 32°–37°N,

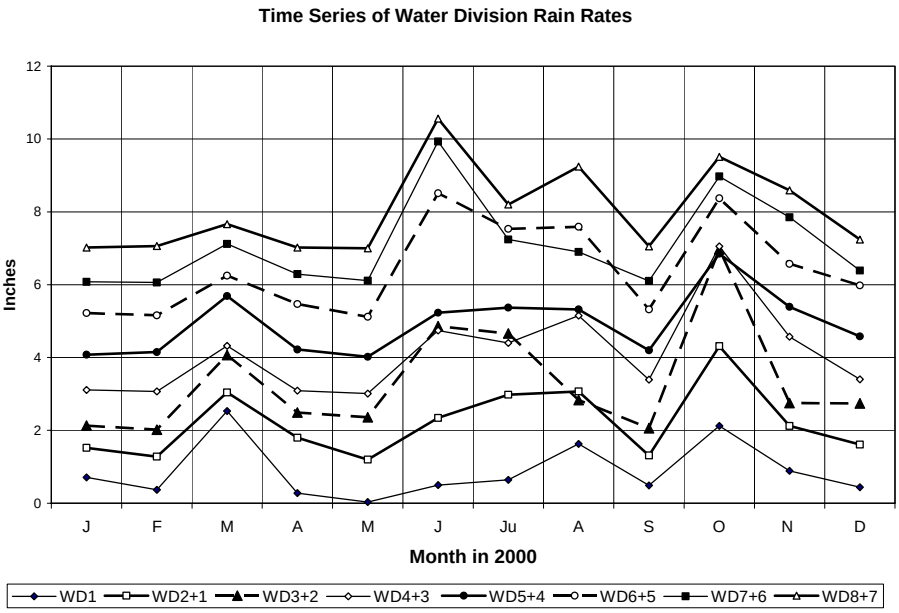

Fig. 3. Time series of monthly rain rates for the eight Water Divisions of New Mexico.

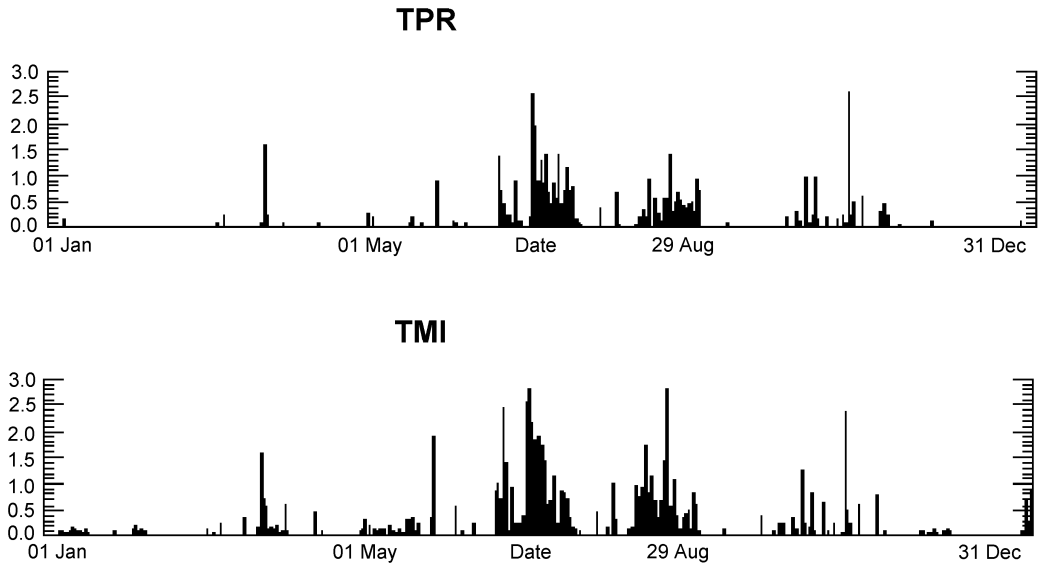

Fig. 4. Time series of the V5 TRMM daily mission index of TPR and TMI rainfall over New Mexico for 2000. (Figure was produced using the TSDIS Orbit Viewer).

109°–103°W, which corresponds approximately to the boundary of the state of New Mexico. Rainfall contribution due to the small extra portion to the southwest is expected to contribute less than a few percent of the statewide rain rate.

Figure 4 shows the TRMM mission index for TMI and TPR during 2000. This figure is produced using the software TSDIS Orbit Viewer developed by TSDIS (ftp://ftp-tsdis.gsfc.nasa.gov/pub/TSDISorbitViewer/download/README.html).The TSDIS Orbit Viewer was developed for the display of most of the TRMM standard products. The TRMM mission index shows the average rain rate over a $1° \times 1°$ box for each instrument, irrespective of the fraction of sensor coverage. The time series shows the average TRMM mission index for TMI and PR for the region 31°–38°N, 110°–102°W. This time series is not meant to be quantitative, but serves as an indicator of the daily rain events in the general area over New Mexico.

Figure 5 shows the time series of the monthly rain

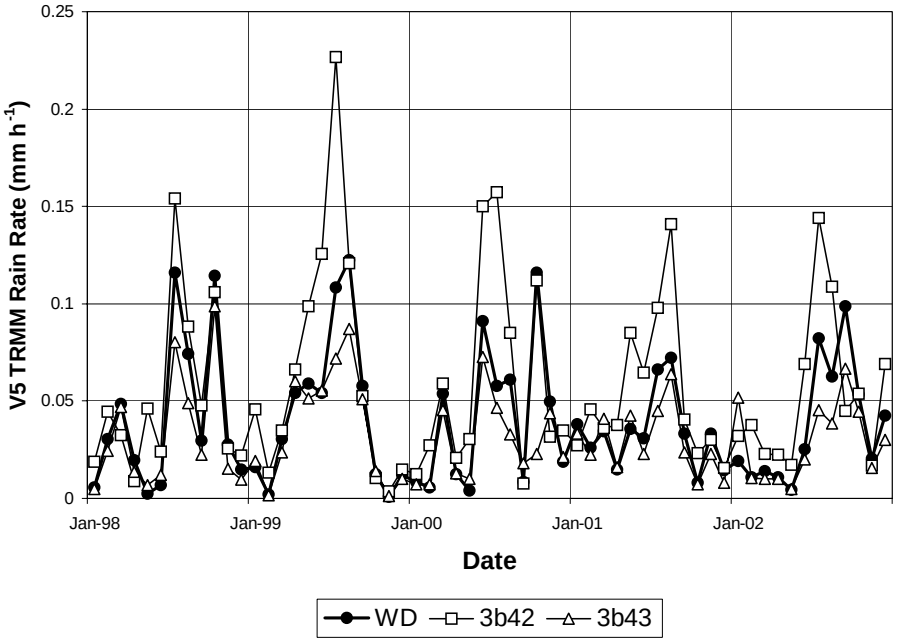

Fig. 5. Time series of monthly V5 TRMM 3B42, 3B43 and WD rainfall over New Mexico for 1998–2002.

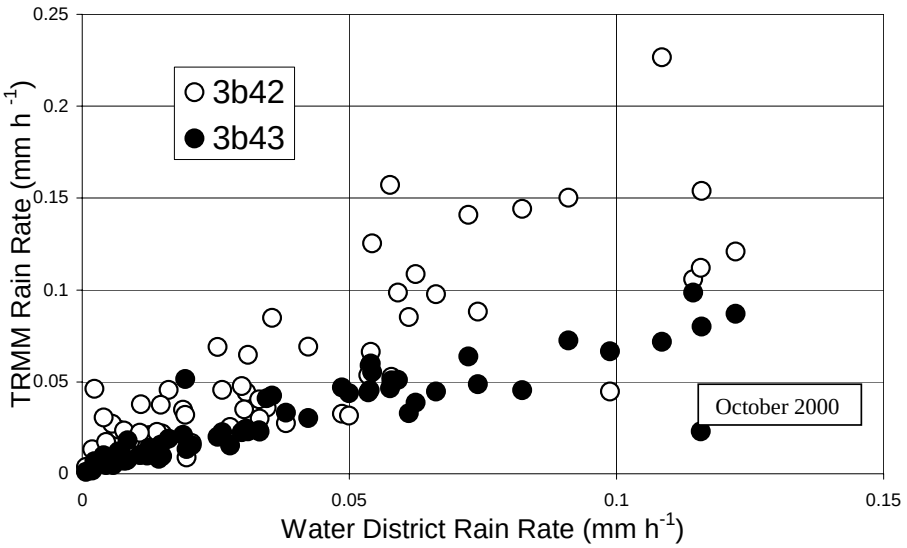

Fig. 6. Scatter diagram of monthly V5 TRMM 3B42 and 3B43 rain rate vs. Water District rain rates (1998–2002). The outlier in 3B43 is identified as October 2000.

rate from 3B42, 3B43 and the WD gauge analyses. 3B43 is very close to the WD estimates, except during the summer months, when 3B43 is lower. The satellite estimates tend to be higher than the WD, especially in the summer. In October 2000, however, WD is significantly higher than the 3B43 estimate, but it closely matches that of 3B42.

Table 3 shows the mean rain rates for each algorithm and the temporal correlation between the TRMM algorithm and WD estimates. The mean rain rate is 0.91 mm d^{-1} for the WDs. Overall, the TMI shows the highest rain rate of 1.49 mm d^{-1}, followed by 3B42, PR, TCA, and 3B43, with rain rates of 1.38, 1.27, 1.07, and 0.75 mm d^{-1}, respectively. All satellite estimates are higher than the WD rain rates in the annual mean. The merged satellite and gauge analysis (3B43) is lower than the WDs. If we consider correlation coefficients greater than 0.80, then a pattern

of algorithm clusters appears. The WD is correlated best with 3B43, and moderately with 3B42 and TCA. 3B42 is correlated with TCA, and there are good correlations among TMI, TPR and TCA. In fact, the best correlation is between TPR and TCA, which is consistent with the result of Shin et al. (2001) who showed no significant difference between TPR and TCA using a paired t-test.

3B43 is a merged satellite and gauge analysis product formed by a weighted average of 3B42 and the gauge analyses. In regions where there are a large number of gauges, the gauge analyses have larger weights. 3B42, by its high temporal and spatial resolution, will be one of the most utilized products for hydrological applications. We examine the differences between 3B42, 3B43 and WDs further. Figure 6 shows the scatter plots of 3B42 and 3B43 vs. WD rain rates. The high biases of 3B42 and the low biases of 3B43 relative to WD are evident. We note an outlier (shown in the diagram) in Fig. 6, which is identified to be the rainfall in October 2000. The WD data in Fig. 3 are further examined to find that the October 2000 rain rates are high over all WDs. The TRMM mission daily rainfall index (Fig. 4) also shows rain events that occurred near the end of month. Since the production of 3B43 has operational constrains, it incorporates gauge analyses provided by either CAMS or GPCC. In most cases, CAMS is used for initial processing. It is suspected that the rain events that occurred at the end of the month were not included in the CAMS analysis, thus they were not reflected in the V5 3B43.

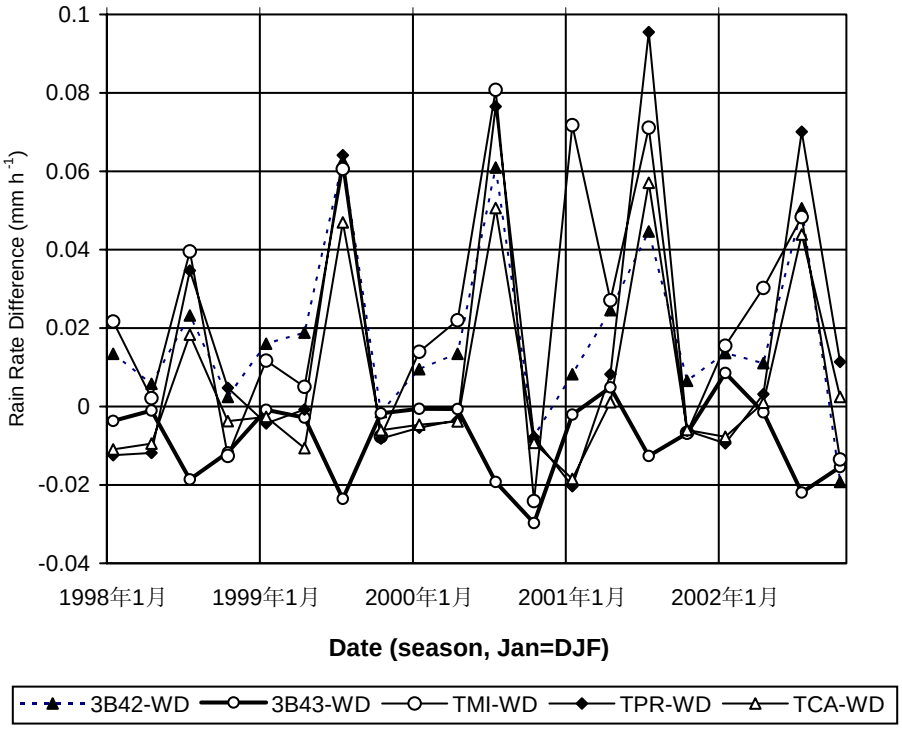

Fig. 7. Seasonal differences between V5 TRMM algorithms and WD rain rates.

Table 4. Annual and seasonal percent biases between V5 and V6 TRMM algorithm and WD rain rates. Percent bias=(TRMM-WD)/WD. V6 biases appear in parentheses. The significance of the differences is tested using a two-sample unequal variance paired t-test. Differences significant at the 95% level appear in bold.

TRMMWD	WD (mm h^{-1})	3B42-WD	3B43-WD	TMI-WD	TPR-WD	TCA-WD
Annual	0.038	**45%**	**–20%(–21%)**	**58%(46%)**	**36%–(7%)**	16%(3%)
DJF	0.016	**76%**	**–20%(–25%)**	**167%**(17%)	**–64%(–70%)**	**–55%(–59%)**
MAM	0.027	55%	0%(−9%)	65%(57%)	−3%(−31%)	−16%(−27%)
JJA	0.069	**70%**	**–28%(-27%)**	**87%(97%)**	**99%**(30%)	**63%(44%)**
SON	0.044	−9%	−30%(−17%)	−29%(−20%)	−3%(−28%)	−10%(−17%)

To provide statistics that are not biased by TRMM sampling, seasonal means are computed. Figure 7 shows the seasonal difference between the TRMM algorithms and WD. The seasonal dependence of the biases of the algorithms is evident. The satellite-only algorithms tend to overestimate the WD rain rates, especially for the summer season, and slightly underestimate them for the fall. 3B43, on the other hand, follows closely that of the WDs but is distinctly lower in the summer and fall.

Table 4 summarizes the biases between the TRMM algorithms and WDs. In the annual mean, TMI shows the largest positive bias (58%), followed by 3B42 (45%), PR (36%) and TCA (16%). The merged gauge product 3B43 shows a negative bias (−20%). Seasonally, there is a large bias in DJF followed by the bias in JJA for TMI. However, a negative bias is calculated for the SON season. The seasonal pattern of 3B42 is very similar, except the magnitudes of the percent biases are smaller. Both TPR and TCA show large positive biases in JJA and negative biases in DJF. The biases in the other seasons are smaller. The percent biases of 3B43 are fairly uniform throughout the seasons at 20%–30%. The MAM bias is lowest.

To quantify the differences, we computed paired t-test between the TRMM algorithms and WD gauge analysis as follows (Chang et al., 1995):

$$t = m[z]/\{\sigma(z)/n^{12}\}\,,$$

where $m[z]$ is the sample mean difference between the two algorithms and $\sigma(z)$ is the sample variance of the estimates of z (Bulmer, 1979). The null hypothesis that $t = 0$ is tested against a two-tail distribution with zero mean. Differences that are significant by this test are marked in bold in Table 4. According to the t-test, TMI and 3B42 are significantly different from the WD analyses. While 3B43 has a low bias in all seasons, the differences are not judged to be significant. Seasonally, all satellite algorithms are significantly higher in summer (JJA), but TPR and TCA have a low bias the winter (DJF). Interestingly, all algorithms show negative biases in the fall. None are statistically significant, however.

3.2 *V6 results*

We computed the same statistics using V6 data. Figure 8 shows the spatial distribution of rain rates from V6 3B42 and 3B43. When compared to Fig. 2, the V6 data show much finer structure, which is introduced by the merging of satellite products. There is practically no difference between 3B42 and 3B43 on the monthly scale, which is consistent with the 3B42 design. The rain rate distribution also shows a resemblance to topography.

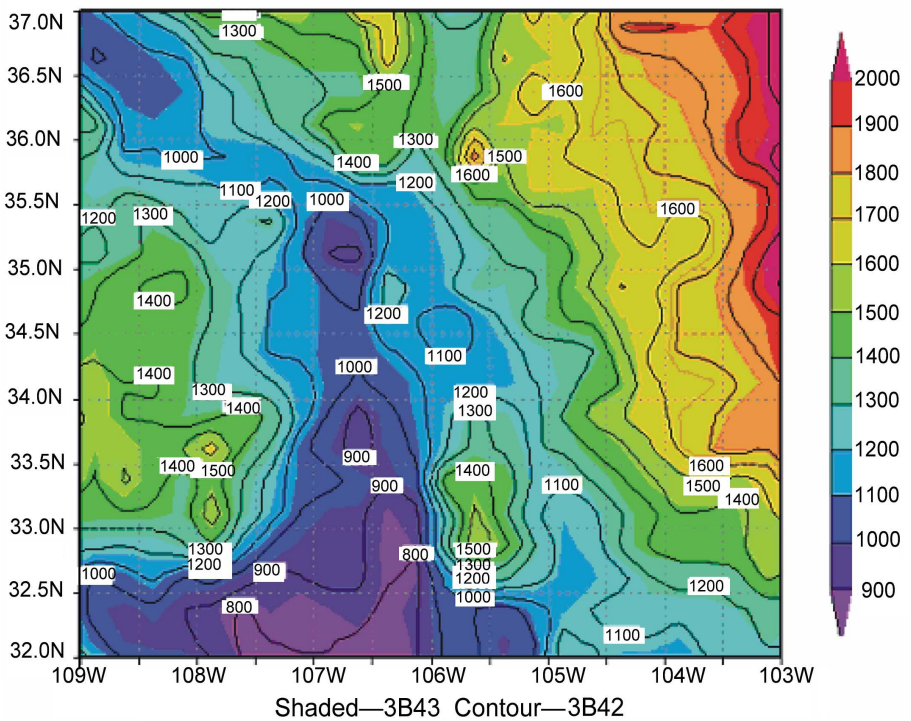

Fig. 8. Same as Fig. 2, except for TRMM V6 algorithms.

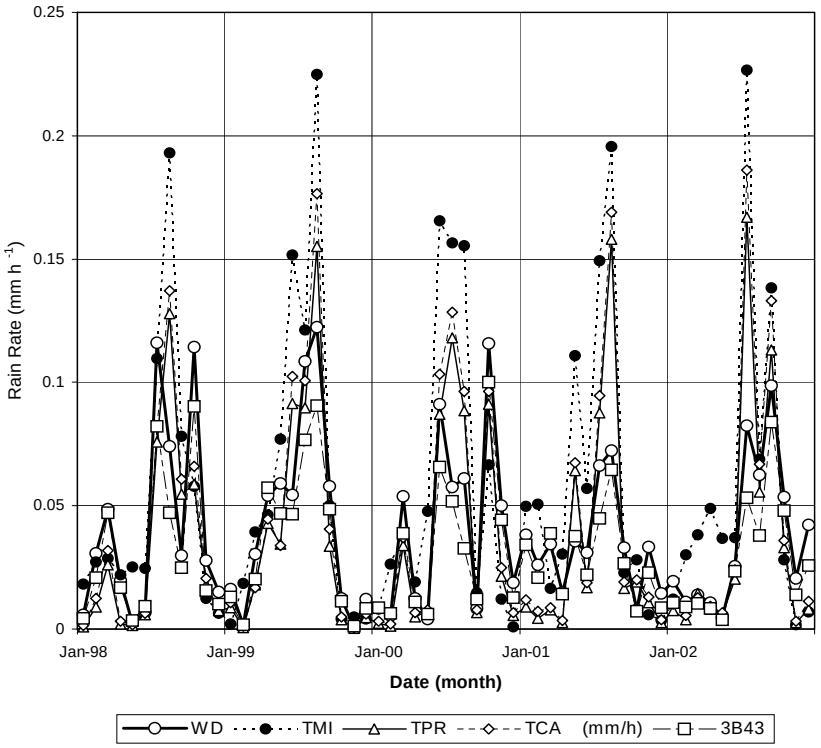

Fig. 9. Time series of monthly V6 TRMM algorithm and WD rain rates.

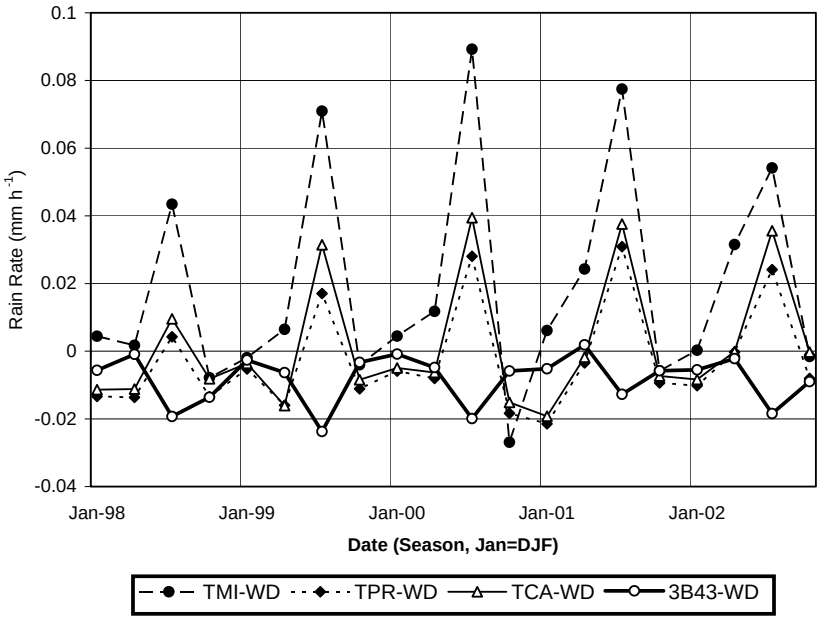

Fig. 10. Same as Fig. 7 but for V6 TRMM data. The plot for monthly 3B42 is omitted as it is almost identical to 3B43.

Overall, the TRMM V6 rain rates decreased by about 7.4%, 31%, 10% and <1% for TMI, TPR, TCA and 3B43 in this region. Figure 9 shows the time series of monthly rain rates of the V6 TRMM and WD rain rates and Fig. 10 shows their difference. An examination of the time series of 3B43 shows an increased rain rate for October 2000, reflecting the improved quality of the reprocessed V6 data. In fact, all V6 TRMM esti-

mates are quite consistent with each other and the WD estimates, thus eliminating the October 2000 outlier in Fig. 6. The TPR and TCA monthly rain rates track each other very well and are almost indistinguishable.

The correlations between monthly WD and V6 TRMM algorithms are computed and summarized in Table 3 (in parenthesis). There are improvements in the correlation between WD and the TRMM algorithms and among the TRMM algorithms. The correlations between the TRMM satellite-only algorithms increased to over 0.95, whereas the correlation between WD and the merged satellite and gauge analysis 3B43 improved to 0.97.

It is instructive to compare the difference between the TRMM V5 and V6 and the WD rain rates. The V6 statistics are included in Table 4 (in parenthesis). Similar t-statistics are computed. While the V6 TMI remains significantly higher than WD in the annual case, there is a reduction in the winter V6 TMI and summer TPR rainfall differences from WD in these seasons. The two seasonal differences are now insignificant by the paired t-test.

4. Summary and discussion

The comparison of five years of monthly average V5 TRMM algorithms with Water District Data over New Mexico shows that all satellite-only algorithms give higher values than the WD gauge estimates. Rainfall variations in the WDs tend to vary in phase, with the best correlation occurring between neighboring WDs. Time series analyses show that monthly average level 2 satellite algorithms (TPR, TMI, and TCA) tend to show high correlations with each other while algorithms 3B42, 3B43, and TCA are better correlated to WD. This is probably related to the sampling of the TRMM satellite sensors. The high correlation between TCA and 3B42 reveals the dependency of V5 3B42 on TCA. The high correlations between monthly 3B42, 3B43 and WD probably reflect the effect of increased sampling by geosynchronous satellite data.

The merged satellite and gauge product (3B43) is consistently lower than the WD estimates, especially in the summer, although a paired t-test shows that such a difference is statistically insignificant. Some of the discrepancies are attributed to the non-inclusion of rain events in the operational CAMS analysis (October 2000 outlier), though these are corrected in the V6 product. We examined GPCC rain rates over the same region and found high correlation between the gauge analysis and GPCC estimates. The five-year average GPCC rain rate is 0.66 mm d^{-1}, which is less than the WD average of 0.91 mm d^{-1}. This can be compared to the average rain rates of 0.75 mm d^{-1} for 3B43 and 1.38 mm d^{-1} for V5 3B42. The number of gauges in the GPCC analysis is approximately 18 for this region, which is lower than that used in the WD analyses. The number of GPCC gauges can be obtained using the TOVAS. The WD analyses have at least 40 gauges in this region since there are at least 5 gauges for each district, hence WD is expected to provide better sampling compared to the GPCC monitoring product. The case of the October 2000 outlier is further vindicated by the V6 3B43 data, which incorporate the GPCC gauge analyses.

There is no significant difference between TPR and TCA for both V5 and V6. This is consistent with earlier studies (Shin et al., 2001; Chiu et al, 2005b). Results from a paired t-test show that V5 TPR and TMI are significantly higher than WD, especially in the summer season. Evaporation of raindrops below the cloud base (virga) may play an important role in the large biases in the summer. In the V6 TPR, however, a surface rain rate is estimated. This parameter takes into account the decrease of the rain rate below the cloud base. This surface rain rate is a better estimate of the actual rain rate reaching the surface than the V5 near-surface rain, and hence it compares better with the WD data. Since the incorporation of water vapor, cloud liquid water and molecular oxygen attenuation increases the TPR rain rate, the correction for the below-cloud-base rain rate is the only mechanism for lower rain rate estimates. With this correction, there is no significant difference between the V6 TPR and WD summer rain rates.

The high bias of V5 TMI in the wintertime may be attributed to the presence of excessive ice scattering or the poor retrieval over ice surfaces. A case in point is the high TMI rain rate in the winter of 2001. The product 3G68 includes rain pixels that may be ambiguous, which can cause the large bias in the wintertime. The development of a land-specific TMI algorithm and an improved land mask is implemented for the V6 TMI algorithm. With better screening of surface pixels, the number of ambiguous pixels is reduced. This leads to wintertime TMI rain rates that are substantially lower, especially for the winter of 2001.

Our results also show a reversal of seasonal biases of TPR (negative bias in winter and positive bias in summer). Chiu et al. (2005b) showed that while TMI is higher in this region overall, TPR is higher than TMI in the summer. Seasonal differences of the source of moisture and cloud type may contribute to the difference in drop size that causes the seasonal biases.

Gauge estimates are also prone to measurement and sampling errors. Major measurement errors include those due to wind field deformation above the orifice (2%–10%), loss from wetting on internal walls of the collector (2%–10%) and loss due to evaporation from the container (0–4%) (Sevruk, 1985; Legates and Willmott, 1990). Fuchs et al. (2001) proposed an

event-based correction for synoptic precipitation observation. The event-based correction is generally less than the other operational procedures. Results show that the event-driven correction values are smaller by about 3%–10% for tropical field experiments (GAME and LBA) that are more appropriate to TRMM algorithms (Rudolf and Rubel, 2004). Rudolf and Rubel (2004) also quoted that empirically determined sampling errors for monthly rainfall over an area of 56000 km^2 are about 3%–5% for 24 gauges. Our study area is approximately $5^\circ \times 6^\circ$, hence it is larger than 56000 km^2. Using the sampling error estimate as our lower bound, and assuming that all the above-mentioned errors are independent, the overall monthly error is estimated to be about 20%–30%. If we applied this criterion to Table 4 for seasonal statistics, it would be consistent with results using the paired t-tests.

The success of TRMM, now in its seventh year of operations, shows great potential for the TRMM follow-up mission, the Global Precipitation Mission (GPM) scheduled for a 2010 launch. The GPM concept consists of a mother satellite with an improved radar and TRMM-like sensor on board, accompanied by microwave sensors on board eight other satellites. This constellation of satellites is capable of delivering roughly 3-hourly microwave-based precipitation estimates, which are better suited for many hydrological applications. The continuation of TRMM, if approved by both the U. S. and Japanese agencies, will extend the TRMM satellite life till 2010, thus providing a possible overlap of TRMM and the GPM satellite. This continuous, long record of satellite and ground-based precipitation observations will further refine satellite precipitation estimates for operational and climate research applications.

Acknowledgments. The authors thank Dr. R. Adler for his continued interest and support. This work was partially supported by NASA's Tropical Rainfall Measuring Mission program and the Hydrology Cluster of the NASA/Federation Earth Science Information Partnership. The TRMM data were processed by the TRMM Science Data and Information System (TSDIS) using algorithms developed by the TRMM Science team, and were distributed by the Goddard Space Flight Center Earth Science Enterprise Distributed Active Archive Center (GES DAAC). Water District data were provided by NCDC. Some of the analyses were performed using the TRMM On-line Visualization and Analysis System (TOVAS) developed by GES DAAC and the TSDIS Orbit Viewer developed by TSDIS.

REFERENCES

Adler, R., C. Kummerow, D. Bolvin, S. Curtis, and C. Kidd, 2003: Status of TRMM monthly estimates of tropical precipitation. *Cloud Systems, Hurricanes, R. F. and the Tropical Rainfall Measuring Mission*, W. K. Tao and R. F. Adler, Eds., Amer. Meteor. Soc., Boston, MA, 223–234.

Bulmer, M. G., 1979: *Principal of Statistics*. Dover, 252pp.

Chang, A.T. C., L. S. Chiu, and G. Yang, 1995: Diurnal cycles of oceanic precipitation from SSM/I data. *Mon. Wea. Rev.*, **123** 3371–3380.

Chiu, L., Z. Liu, H. Rui, and W. Teng, 2005a: Tropical Rainfall Measuring Mission (TRMM) data and access. *Earth Science Satellite Remote Sensing*, Qu et al., Eds., Springer and Tsinghua University Press. (in press)

Chiu, L., D.-B. Shin, and J. Kwaitowski, 2005b: Surface rain rates from TRMM algorithms. *Earth Science Satellite Remote Sensing*, Qu et al., Eds., Springer and Tsinghua University Press. (in press)

Fuchs, T., J. Rapp, F. Rubel, and B. Rudolf, 2001: Correction of synoptic precipitation observations due to systematic measurement errors with special regard to precipitation phases. *Physics and Chemistry of the Earth, Part B—Hydrology Oceans and Atmosphere*, **26**(9), 689–693.

Haddad, Z. S., E. A. Smith, C. D. Kummerow, T. Iguchi, M. R. Farrar, S. L. Durden, M. Alves, and W. S. Olson, 1997a: The TRMM "Day-1" radar/radiometer combined rain-profiling algorithm. *J. Meteor. Soc. Japan*, **75**, 799–809.

Haddad, Z. S., D. A. Short, S. L. Durden, E. Im, S. Hensley, M. B. Grable and R.A. Black, 1997b: A new parametrization of the rain drop size distribution. *IEEE Trans. Geosci. Rem. Sens.*, **35**, 532–539.

Huffman, G. J., and Coauthors, 1997: The Global Precipitation Climatology Project (GPCP) combined precipitation dataset. *Bull. Amer. Meteor. Soc.*, **78**, 5–20.

Huffman, G. J., and Coauthors, 2001: Global precipitation at one degree daily resolution from multisatellite observations. *J. Hydrometeor.*, **2**(1), 36–50.

Huffman, G. J., R. Adler, D. Bolvin, and E. Nelkin, 2004: Uncertainty in fine-scale MPA precipitation estimates and implications for hydrometeorological analysis and forecasting. 18th Conf. on Hydrology, 11–18 January 2004, Seattle, WA.

Iguchi, Toshio, T. Kozu, R. Meneghini, J. Awaka, K. Okamoto, 2000: Rain-profiling algorithm for the TRMM precipitation radar. *J. Appl. Meteor.*, **39**, 2038–2052.

Kummerow, C., W. Barnes, T. Kozu, J. Shiue, and J. Simpson, 1998: The Tropical Rainfall Measuring Mission (TRMM) sensor package. *J. Atmos. Oceanic Tech.*, **15**, 809–816.

Kummerow, C., and Coauthors, 2000: The status of the Tropical Rainfall Measuring Mission (TRMM) after two years in orbit. *J. Appl. Meteor.*, **39**, 1965–1982.

Kummerow, C., and Coauthors, 2001: The evolution of the Goddard Profiling Algorithm (GPROF) for rainfall estimation from passive microwave sensors. *J. Appl. Meteor.*, **40**, 1801–1820.

Legates, D. R., and C. J. Willmott, 1990: Mean seasonal and spatial variability in gauge corrected, global precipitation. *Int'1 J. of Clim.*, **10**, 111–127.

Liu, Z., H. Rui, W. Teng, and L. Chiu, 2003: Online analysis and visualization of TRMM and QuikSCAT products. Preprint, *12th Conference on Interactions of the Sea and Atmosphere*, Long Beach, California, Amer. Meteor. Soc., Boston.

Meneghini, R., J. A. Jones, T. Iguchi, K. Okamoto, and J. Kwiatkowski, 2004: A hybrid surface reference technique and its application to the TRMM precipitation radar. *J. Atmos. Oceanic Tech.*, **21**, 1645–1658.

Rudloff, W., 1981: *World Climate, Books of the Journal Naturwissenschaftliche Rundschau*, W. Holl, Ed., Wissenschaftliche Verlagsgesellschaft Stuttgart, 632pp.

Rudolf, B., H. Hauschild, W. Ruth, and U. Schneider, 1994: Terrestrial precipitation analysis: Operational method and required density of point measurements. *Global Precipitation and Climate Change*, Dubois and Desalmand, Eds., Springer Verlag, 173–186.

Rudolf, B., and F. Rubel, 2004: Global Precipitation. *Observed Global Climate*, Hantel, M. Ed., Springer-Verlag, (submitted, copy available from http://www.dwd.de/en/FundE/Klima/KLIS/int/GPCC/Reports_Publications/QR/LB11RudolfRubel2-0040715oA.pdf)

Shin, D.-B., L. S. Chiu, and M. Kafatos, 2001: Comparison of the monthly precipitation derived from the TRMM satellite. *Geophys. Res. Lett.*, **28**(5), 795–798,

Simpson, J., R. Adler, and G. North, 1988: A proposed Tropical Rainfall Measuring Mission satellite. *Bull. Amer. Meteor. Soc.*, **69**, 278–295.

Sevruk, B. 1985: Correction of Precipitation Measurements. *Proc. International Workshop on Precipitation Correction Measurements*, Zurich, Switzerland, WMO/IAHS/ETH, 13–23.

Young, C. B., B. R. Nelson, A. A. Bradley, J. A. Smith, C. D. Peters-Lidard, A. Kruger, and M. L. Baeck, 1999: An evaluation of NEXRAD precipitation estimates in complex terrain. *J. Geophys. Res.*, **104**(D16), 19691–19703.